Thallium removal by the montmorillonite biochar composite: insights and environmental implications

Eric Cyubahiro[a,b], Zhuanxi Luo[a,c,]*, Alexis Kayiranga[a,b], Theogene Habumugisha[a,b], François Nkinahamira[a,b], Jean Claude Ndayishimiye[a,b,e], Changzhou Yan[a], Jianhua Guo[a,b], Zhenhong Wang[d]

[a]*Institute of Urban Environment, Chinese Academy of Sciences, Xiamen 361021, China, Tel. 13328784636;*
email: zxluo@hqu.edu.cn/zxluoire@163.com (Z. Luo), Tel. 13023902659; email: eric@iue.ac.cn (E. Cyubahiro),
Tel. 15960243524; email: sbony2sbony@yahoo.com (A. Kayiranga), Tel. 15659260050;
email: habumugisha@iue.ac.cn (T. Habumugisha), Tel. 15606097675; email: Francois@hit.edu.cn (F. Nkinahamira),
Tel. 159 6023 5991; email: 6420210004@smbu.edu.cn (J.C. Ndayishimiye), Tel. +86-592-6190993;
email: czyan@iue.ac.cn (C. Yan), Tel. 13063073858; email: 2533541270@qq.com (J. Guo)
[b]*University of Chinese Academy of Sciences, Beijing 100049 China*
[c]*College of Chemical Engineering, Huaqiao University, Xiamen 361021, China*
[d]*College of Chemistry, Chemical Engineering and Environment, Fujian Province Key Laboratory of Modern*
Analytical Science and Separation Technology, Key Laboratory of Pollution Monitoring and Control,
Minnan Normal University, Zhangzhou 363000, China, Tel. 13799816087; email: zhhwang1979@163.com (Z. Wang)
[e]*Faculty of Biology, Shenzhen MSU-BIT University, Shenzhen 518172, China*

ABSTRACT

Thallium (Tl) contamination is of main concerns due to its high toxicity in the environment. To date, Tl adsorption is critical but limited by less knowledge on the designing and application of cost-effective and potential materials for its removal. In this work, a montmorillonite biochar composite (MMT-BC) was synthesized from biochar (BC) and montmorillonite (MMT). It was characterized to know its Tl's adsorption mechanisms and was evaluated for its ability to remove Tl through batch adsorption experiments. The results showed that MMT-BC had a higher Tl removal rate than BC and MMT. The adsorption fitted well the Freundlich model with the highest adsorption capacities of MMT-BC (79.7 µg/g), which was higher than 69.8 µg/g of BC and 67.1 µg/g of MMT at 800 µg/L of the initial concentration. Ion exchange, electrostatic attraction, and complexation were the main processes influencing Tl adsorption onto MMT-BC. Furthermore, MMT-BC manifested a higher removal percentage of 95.85% under high ionic strength and high selectivity of 95.15% and 93.66% towards Tl in co-existence with Cu^{2+} and Pb^{2+}, respectively. The desorption percentage was 89.4%, 83% and 98.9% for BC, MMT and MMT-BC, respectively. Therefore, our findings highlighted that MMT-BC is a potential material for controlling Tl contamination in the environment.

Keywords: Thallium; Montmorillonite; Adsorption; Biochar; Composite

* Corresponding author.

1. Introduction

Heavy metals contamination is a worldwide issue of primary concern. They enter the environment through various sources such as industries, motor vehicle emissions, construction, mining, and the application of pesticides and fertilizers [1,2]. They are highly prioritized because they can persist in soils and aqueous media and do not undergo biodegradation [3]. Thallium (Tl) is one of heavy metals present in the environment without any biological function in plants and animals' bodies [4]. The United States Environmental Protection Agency (USEPA) has recognized Tl among 13 important heavy metal contaminants, which are highly toxic [5]. Additionally, Tl is considered as principal pollutant in many countries [6]. As known, Tl has been pronounced to have its source from mining, metallurgy, coal combustion, and the discharge of wastewater from various industries [7,8]. It is strongly toxic, responsible for serious harms to animals and human bodies through the food chain [9,10]. To reduce the health risks associated with Tl contamination, the USEPA proposed the maximum acceptable limit because its contamination was increasing, especially in developed countries [11]. Hence it is highly warranted to conduct advanced research aiming to remove Tl from the environment.

Considering its efficacy, low cost, and ease of operation, the adsorption method has been selected to remove Tl [12,13]. Through adsorption, Tl can be accumulated or stabilized in the pores and on the surface of adsorbents, thereby decreasing their mobility and bioavailability [14], and in most cases, yield a well-treated effluent [15]. However, Tl is generally found in coexistence with other heavy metals in various aqueous solutions, creating the competition during its adsorption due to they have almost or the same adsorption sites [16]. Nowadays, different novel and economical adsorbent materials have been suggested for removing Tl [9,11]. Each adsorbent presents benefits and drawbacks; the high cost, low adsorption capacity, and prolonged equilibrium time are among the main constraints for most adsorbents [17,18]. Therefore, it is highly needed to develop a novel, low-cost, and practical material which is rapid and has high adsorption capacities of Tl.

Biochar is a carbon-rich material produced by thermal decomposition (pyrolysis) of organic materials, including agricultural bio-waste, forest residues, and animal wastes in oxygen-limited conditions [19,20]. Its physicochemical characteristics such as functional groups, large surface area, high porosity, cation exchange, low cost and availability make it an adsorbent of superior choice for heavy metals removal [21]. For instance, some Tl ions are immobilized in pores of biochar, exchange with biochar cations, other form complexes with oxygen-containing functional groups like –COOH, C=O, and –OH and electrostatic attraction positive charges of Tl and negative charges of biochar [22]. Bamboo has been a good precursor for biochar production [23]. Similarly, montmorillonite (MMT) is among clay minerals reported as one of plentiful resources on the earth. It has versatile utilization, including heavy metals remediation due to its low cost and wide availability, high specific surface area, firmness layered structure, cation exchange capacity, etc. [24,25]. Previous studies

have used bamboo-derived biochar (BC) [26], and others used montmorillonite clay [27] to remediate heavy metals. While materials with rough surfaces such as BC generally exhibit a possibility of accumulating large amount of heavy metals [28,29], materials with more regular shapes such as MMT may increase the amount of oxygen-containing functional groups, exchangeable cations to improve the efficiency of capturing the contaminant[30,31]. Thus, complementing both material types could improve the adsorption capacity and efficiency of the adsorbent. However, to the best of the authors' knowledge, little information is available on the potential of montmorillonite biochar (MMT-BC) to remove Tl in the environment.

Accordingly, the objectives of this study were (1) to investigate the ability of MMT-BC to remove Tl from the aqueous environment, (2) to explore the potential mechanisms underlying Tl adsorption onto MMT-BC (3) to examine the competitive adsorption of Tl in coexistence with other heavy metals onto MMT-BC, and (4) to discuss its environmental implication and application. The obtained results will provide a deep understanding of designing a cost-effective adsorbent material from MMT and BC and its application for Tl removal in the environment.

2. Materials and methods

2.1. Materials

BC was bought from the Xinshiji Company in Zhejiang Province, China. MMT (CAS: 1318-93-0) and Tl NO_3 (CAS: 10102-45-1) were purchased from Sinopharm Chemical Reagents Co., Ltd., China. To get the Tl stock solution of 200 mg/L, the appropriate amount of $TlNO_3$ was dissolved in Milli-Q water (Millipore Corp.). The following required solutions of varying levels of Tl have been prepared by diluting the stock solution. A pure standard solution containing 1,000 mg/L of Tl was obtained from China's National Center of Analysis. Chemicals such as HNO_3, NaOH, and $NaNO_3$ used in this study were of analytical grade, acquired from Sino Pharm Chemical Reagent Co., Ltd. All experiments were accomplished using Milli-Q water (Millipore Corp.).

Additionally, MMT-BC was prepared from BC and MMT as described below. Firstly, 5 g of MMT was added to 500 mL of deionized water to prepare the clay suspension. To obtain a good mixture, the suspension spent 60 min in an incubator shaker (ZHWY-2102C, China), and then 1 g of biochar powder was added and shaken again for 90 min. Afterward, the feedstock was removed from the mixture and oven-dried at 105°C for 24 h. In this study, no pyrolysis was involved because it is non-economic and may stimulate the activation of other reactive compounds in the material [32]. Finally, samples were grounded using an agate bowl, sieved in a 100–200 mesh screen and stored in plastic bags for further experiments. Meanwhile, pure BC and MMT were used as a reference in this study.

2.2. Characterization of adsorbent materials

The pH meter (STARTER3100/F, Ohaus Inc., China) was used to determine the pH values of BC, MMT and MMT-BC using a 1:20 ratio (solid:liquid). Using the pH

values ranging from 3 to 10, the zeta potential of the materials was determined by means of a Zeta PALS analyzer (Malvern Instruments, Malvern, United Kingdom) to find the points of zero charge (pH_{PZC}). The point of zero charge of every sample was determined as previously reported [18]. The C, N, S elements embedded in the tested materials were determined using an elemental analyzer (Elementar Analysensysteme GmbH – Vario MAX, Germany). The percentage of oxygen in the samples was calculated using the formula O% = 100–(N + S + C) %. The exchangeable cations or alkali metals/alkali earth metals such as Ca, K, Mg, and Na were measured using inductively coupled plasma optical emission spectrometry (ICP-OES, PerkinElmer Optima 7000DV, USA).

A scanning electron microscopy (SEM Hitachi S-4800, Tokyo, Japan) was used to observe the morphology and elemental composition of the tested materials in combination with energy-dispersive X-ray spectroscopy (EDS) (Genesis, XM2, FL, USA). The X-ray diffraction (XRD) measurements were taken on a PANAanalytical X'Pert Pro diffractometer with Ni filtered, Cu Kα radiation (=1.54056) to know the BC, MMT and MMT-BC crystallography. Thermo Scientific Nicolet iS10, USA was used to record Fourier-transform infrared spectrometer (FTIR) spectra between the wavelengths of 4,000 and 500 cm^{-1} to determine the functional groups. A mixture of 1.5 mg dried sample and 200 mg KBr was used to pelletise the sample during sample preparation.

On a micromeritics ASAP 2020 instrument, the N_2 adsorption/desorption isotherms were calculated at liquid nitrogen temperature (–196°C) and a relative pressure range of 0.001 to 0.998. Before measurement, the samples were outgassed at 160°C for 12 h under a vacuum of less than 10^{-3} Torr. From the desorption data and in the relative pressure range of 0.05–0.35, the surface area was assessed using the Brunauer–Emmett–Teller (BET) equation [33]. At a relative pressure of 0.995, the total pore volume was calculated using the quantity of N_2 adsorbed. Furthermore, X-ray photoelectron spectroscopy (XPS, Thermo ESCALAB 250 K-Alpha+, Thermo Fisher Scientific Inc., USA) was used to analyze the elemental composition and their valence states on the surface of the materials utilizing Al Kα radiation.

2.3. Sorption experiments

To investigate different environmental parameters influencing the adsorption process, the batch experiments of Tl adsorption onto BC, MMT and MMT-BC were conducted. Fixing the initial concentration of Tl at 100 μg/L, pH of 7, rotation speed of 180 rpm and the volume of 25 mL at room temperature (25°C) for 24 h, the effect of adsorbent dosage was studied as described in supplementary information (section 1). The effect rotation speed and temperature were investigated as shown in supplementary information (section 2 and section 3). Furthermore, the experimental conditions of pH, the initial Tl concentration, contact time, ionic strength, and coexistence with other heavy metals were determined by the obtained results of adsorbent dosage, rotation speed, and temperature. Specifically, the effect of adsorbent dosage was studied in the range between 2–40 g/L; rotation speed was varied

between 50 and 400 rpm, and the temperature between 10°C ± 1°C and 35°C ± 1°C. To assess the effect of pH on the adsorption process, the experimental studies were performed in a pH range from 2 to 10.

Meanwhile, the initial Tl concentration was varied between 200 and 800 μg/L whereas the effect of contact time was studied between 2 and 60 min. Various initial salt (NaNO$_3$) concentrations ranging from 0.001 M to 0.2 M were prepared and used as background electrolytes to evaluate the effect of ionic strength on Tl adsorption. To examine the effect of co-existence, different concentrations (100, 200, and 500 μg/L) of Pb^{2+} and Cu^{2+} were used and a concentration of (100 μg/L) of only Tl was used as control treatment (CK).

Accordingly, unless otherwise specified, experimental tests have been carried out as follows: 0.25 g of adsorbents was melded with 25 mL of Tl (100 μg/L) using centrifuge sealed bottles (50 mL), with a rotation speed of 200 rpm, pH of 7 at 25°C for 24 h, and lastly centrifuged at 3,000 rpm for 10 min. The suspensions have been purified using 0.45 μm filters, and the residual Tl concentration has been determined using inductively coupled plasma mass spectroscopy (ICP-MS, Agilent 7500CX). The quantity of absorbed metal was determined as the difference between the original and concentration of Tl in solution at a particular time per unit of adsorbent mass. The amount of Tl absorbed per unit of adsorbent weight was determined based on Eq. (1). While the removal efficiency was calculated using Eq. (2).

$$q_e = \frac{(C_o - C_t) \times V}{m} \tag{1}$$

$$\text{Removal efficiency} (\%) = \frac{(C_o - C_t)}{C_o} \times 100 \tag{2}$$

where q_e is the adsorption capacity (μg/g), C_o and C_t are the initial Tl concentrations and concentrations at time t, respectively, V is the volume of the aqueous solution (L) and m is the mass of adsorbent materials (g).

After adsorption experiment using 100 μg/L, the samples were filtered and oven-dried at 100°C for 12 h, disseminated into the background electrolyte of Milli-Q water (pH = 3) using 0.5 M HNO$_3$ for 4 h.

$$\text{Desorption} (\%) = \frac{C_{\text{des}}}{C_o} \times 100 \tag{3}$$

where C_{des} is the desorbed Tl concentration (μg/L) and C_o (μg/L) is adsorbed Tl concentration.

2.4. Fitting models for kinetic and isotherm studies

The pseudo-first-order and pseudo-second-order models were used to analyze the adsorption kinetic using Eqs. (4) and (5).

Pseudo-first-order kinetic model: $\ln(q_e - q_t) = \ln q_e - k_1 t$ (4)

Pseudo-second-order model: $\dfrac{t}{q_t} = \dfrac{1}{q_e}t + \dfrac{1}{k_2 q_e^2}$ ⠀⠀⠀(5)

where k_1 (1/min) and k_2 (g/μg min) are rate constants of the pseudo-first-order and pseudo-second-order models where q_e (μg/g) and q_t (μg/g) are the amounts of Tl adsorbed at equilibrium and time t, respectively.

To study the isotherm adsorption, Langmuir and Freundlich models fitness were used following Eqs. (6) and (7) as described below:

Langmuir model: $\dfrac{C_e}{q_e} = \dfrac{1}{q_m}C_e + \dfrac{1}{q_m}k_L$ ⠀⠀⠀(6)

Freundlich model: $\ln q_e = \dfrac{1}{n}\ln C_e + \ln K_F$ ⠀⠀⠀(7)

where C_e (μg/L) is the concentration at equilibrium; q_e (μg/g) is the equilibrium adsorption capacity; q_m (μg/g) is the theoretical maximum sorption capacity, and K_L (L/μg) and K_F (mg/g (L/mg)$^{1/n}$) are the Langmuir and Freundlich adsorption constants, n symbolizes a heterogeneity factor. For the Langmuir model, q_m and K_L are generated by the slope and intercept of the linear plots of C_e/q_e vs. C_e.

2.5. Statistical analysis

All the experiments were conducted in triplicate. The mean values were used to present analytical data, and error bars were indicated to display the highest deviation from average values. Statistical significance was performed using a One-Way ANOVA in SPSS 17.0, and measured values considered significant at $P < 0.05$ level.

3. Results and discussions

3.1. Characterization of the adsorbents

3.1.1. pH and point of zero charge

The pH of BC, MMT and MMT-BC were 8.9 ± 0.5, 9.7 ± 0.5 and 10.0 ± 0.5, respectively. The point of zero charge (PZC) is referred to the pH at which the number of negative charges on the adsorbent surface is equal to the number of positive charges. At pH values below pH$_{PZC}$, the adsorbent's surface is positively charged whereas at pH values above pH$_{PZC}$, the surface is negatively charged favoring cation adsorption [18]. The zeta potentials of all the three studied materials decreased with increasing pH and were all negative, varying in the range of –18 and –38.2 mV (Fig. 1a). Negative charges will enhance the adsorption of positively charged Tl and inhibit the risks of aggregation of adsorbent materials in the solution. PZC values of the materials were 7.4, 8.0, and 8.5 for MMT, MMT-BC, and BC, respectively as shown in Fig. 1b.

3.1.2. Elemental composition (%) of samples by CNS

In this study as presented in Table S1, O was more than other elements (N, C, and S). The sample MMT had a very low amount of carbon mainly because, naturally, MMT contains low carbon content [34]. The O/C and (O+N+S)/C shows the dehydration degree. Their ratios were greater in MMT and MMT-BC than in BC, indicating the higher carbonization degree of the later. Generally, the C content depends on feedstock material and temperature. It was low in MMT-BC mainly due to its high content of metal elements from MMT and low carbonization degree [35]. The presence of alkali and alkali earth metals including Ca, K, Mg, and Na in the adsorbents was tested and their results are presented in Table S2.
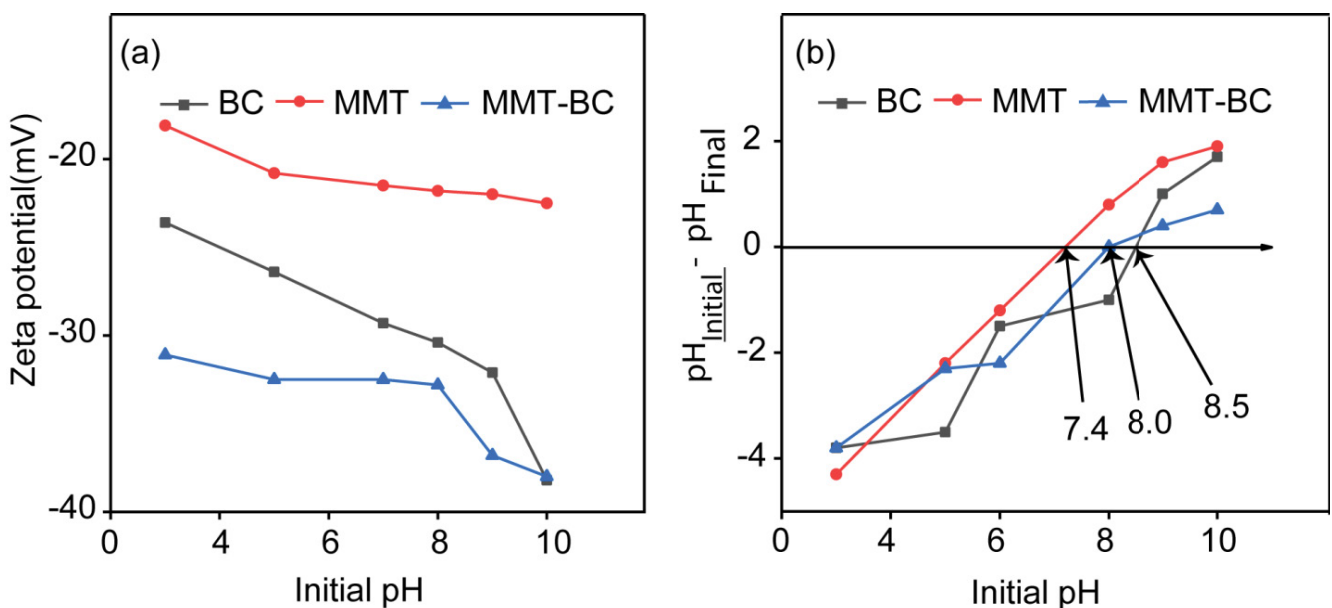
Fig. 1. Zeta potential (a) and point of zero charges (b) of BC, MMT and MMT-BC.

3.1.3. Morphology and elemental analysis of adsorbents

The analysis of SEM-EDS data was accomplished before and after Tl adsorption (Fig. S1). The surface of MMT-BC was more irregular and rough than BC and MMT, suggesting the high possibility of accumulating Tl. The BC also presented rough surfaces, resulting from volatile compounds removal during pyrolysis. Contrarily, the MMT surface had regular shapes. The high peaks of silicon, aluminum, sodium, calcium, magnesium, and iron, which are characteristic of the elemental composition of clay minerals observed on the EDS images of MMT-BC, confirmed the existence of MMT in the composite (Fig. S1b). On the other hand, a high peak of Si was observed in MMT-BC than in MMT, which was assigned to the introduction of quartz (SiO_2) reported being the common biochar component [36]. During MMT-BC preparation, MMT increased the amount of oxygen-containing functional groups, immediately increasing the adsorption sites for Tl [37]. After adsorption, there was a formation of new peaks of Tl which was attributed to the accumulation of Tl on the BC, MMT and MMT-BC (Fig. S1b).

(XRD) configurations of BC, MMT, and MMT-BC are presented in Fig. S2. The peaks observed at 2θ values of 22, 26.5, and 36.10 approved the porous structure of these adsorbent materials. As shown in the figures, no false diffractions confirm the crystallographic purity of materials under investigation [38]. The XRD results strongly agree with the SEM-EDS findings, proving that the production method used in this study has effectively embedded BC into MMT surface.

3.1.4. FTIR analysis

The FTIR analysis was performed between 4,000 and 500 cm^{-1} before and after Tl adsorption to detect the potential binding sites of Tl on the adsorbent surfaces (Fig. S3). For BC, the peaks at 3,432 cm^{-1} corresponded to –OH stretching vibrations, while the bands at 1,648 and 1,037 cm^{-1} are assigned to C=O and C–O stretching of ether groups, respectively[39]. The bands located at 3,450 and 1,646 cm^{-1} on MMT spectrum belong to –OH stretching vibrations and –OH bending mode, respectively [40]. Other bands located at 1,089, and 1,039 cm^{-1} on the same spectrum correspond to Si–O–Si stretches. Moreover, in the range of 500 and 1,000 cm^{-1}, several components such as Si–OH and Al–OH located at 792, 626 and 526 cm^{-1} are the primary functional groups of MMT [41]. The strong bands at 3,631 and 3,448 cm^{-1} are attributed to hydrogen-bonded H–O–H stretching vibrations as representative hydroxyl groups in MMT-BC. The band at 1,646 cm^{-1} confirmed the presence of C=O ether groups in MMT-BC, while the bands located at 1,091 and 1,037 cm^{-1} belong to Si–O–Si layered vibrations stretches MMT. Again, different functional groups of Si–O and Al–OH were observed between 500 and 1,000 cm^{-1} located at 792, 626 and 526 cm^{-1} because MMT is the main component of the composite. The functional groups observed on the surface of MMT-BC, extreme peaks of –OH, are expected to stimulate the adsorption of Tl [42].

After Tl adsorption, the observed peaks were almost the same as before, with minor changes in wavenumbers from higher to lower positions (Fig. S3). For instance, the peak corresponding to –OH has shifted from 3,432 to 3,417 cm^{-1}, 3,450 to 3,430 cm^{-1} and 3,448 to 3,432 cm^{-1} for BC, MMT and MMT-BC, respectively. The reduction in peak position has been observed on other functional groups proposing that there has been an interaction between Tl ions and the surface of the adsorbents. It also approves that the functional groups have played an essential role during Tl ions bonding [43].

3.1.5. Porosity and surface area analyses

The results from this study manifested that the specific surface area (SSA) and pore volume of MMT-BC is higher compared to that of BC due to the incorporation of alkali metals like Na in it (Table S3). However, the SSA of MMT-BC reduced compared to MMT, probably due to the clogging of pores of MMT by BC [44]. Moreover, as indicated by their average pore size results (Table S3), the three adsorbents were mesoporous, showing that they can increase the adsorption spaces for Tl, and fitted the type III according to the IUPAC classification as indicated by their Nitrogen adsorption–desorption isotherms (Fig. S4). Though no pyrolysis was involved in this study, the SSA, pore-volume and pore diameter of MMT-BC are comparable with the previous findings [30,45].

3.1.6. XPS observation

The evaluation results from XPS clearly showed the chemical states of three adsorbents, BC, MMT, and MMT-BC (Fig. 2). For BC and MMT-BC (Fig. 2a and c), the surface of the materials presented two prominent peaks located at 284.30 (C1s) and 531.4 eV (O1s). The C1s spectra fitted components such as C–C/C–H, C–COOX, C–OH, COO–, and COOH species that may be assigned to $C_{10}H_8$ [46]. The presence of C in MMT-BC mainly comes from biochar due to carbonization during composite preparation. In the O1s spectra, peaks were expansive, which indicates the existence of various chemical states of oxygen. They consisted of organic oxygen (O in carboxyl, carbonyl, alkoxyl, or ether groups) and inorganic oxygen (O in iron oxides) in biochars and iron or aluminum-containing oxides or other surface hydroxyls [47] and silicon oxides (SiO_2) but also from OH groups in MMT. In Fig. 2b, the MMT showed spectra with two prominent peaks located at 101.10 ev (Si) and 529.90 eV (O), which probably corresponds to SiO_2 [44] and OH of the montmorillonite, respectively [45].

3.2. Results of batch experiments

3.2.1. Effect of pH

Tl absorption onto BC, MMT and MMT-BC increased with increasing pH from 2.0 to 10.0. The highest adsorption percentage of 99.8%, 97.4% and 99.9% for BC, MMT, and MMT-BC, respectively, occurred at a pH of 10 (Fig. S8). Specifically, at lower pH, the functional groups of BC, MMT and MMT-BC can be protonated to some extent. Subsequently, this protonation increased H^+ ions, and the surface of the adsorbents become positively charged, which could result in repulsion with positively charged Tl. On the
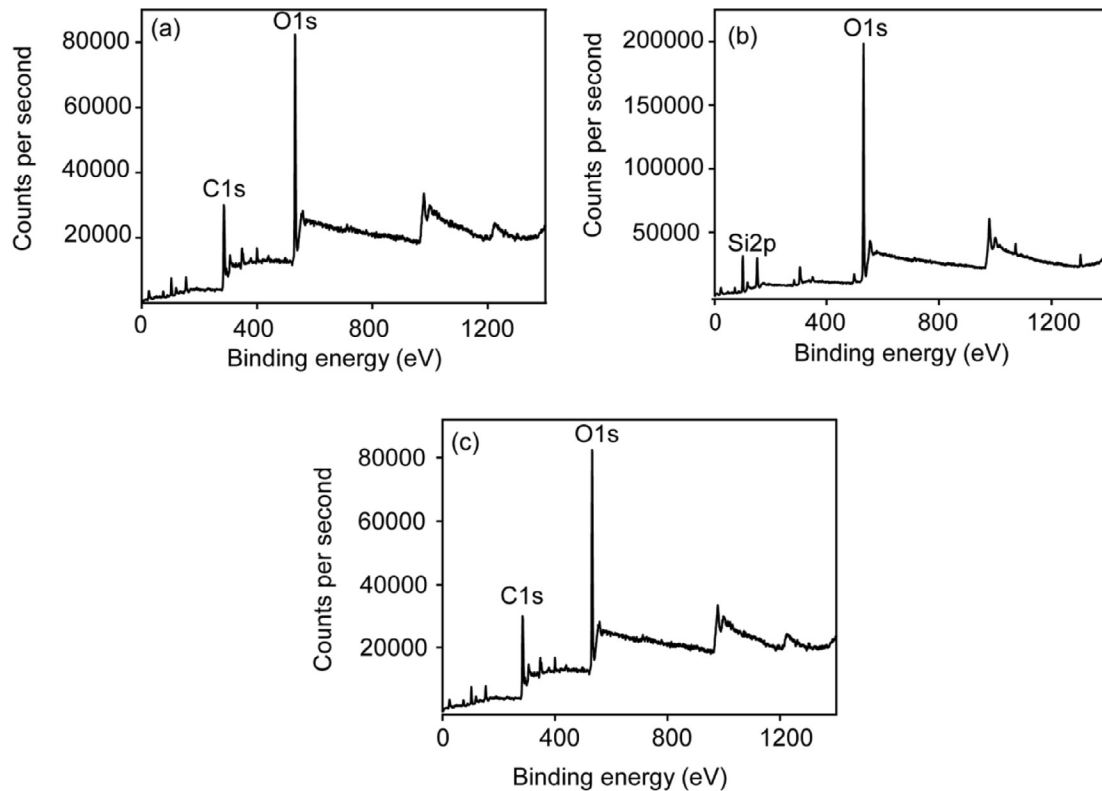
Fig. 2. XPS full survey of BC (a), MMT (b) and MMT-BC (c).

other hand, when the solution pH is greater than the pH_{PZC}, the same functional groups (active sites) are deprotonated to create negative charges on the surface of the adsorbents. Consequently, the deprotonation enhanced the binding of positively charged Tl ions and increased the attraction between positively charged Tl and the negative surface of the adsorbents [43]. Thus at higher pH, the three tested adsorbents presented high Tl removal, particularly MMT-BC. But also, for the case of MMT and MMT-BC, it can be linked with the high release of cations of MMT at higher pH values, then favoring Tl adsorption through ionic exchange [44].

3.2.2. Adsorption isotherm and capacity

The results clearly manifested that an increase in the initial concentration of Tl was followed by an increase in adsorption capacity (Fig. 3). The highest adsorption capacity was 69.8, 67.1, and 79.7 µg/g for BC, MMT, and MMT-BC, respectively at 800 µg/L of initial concentration. At low initial concentration Tl removal was very quick due to the availability of specific sites and low concentration of the adsorbate, but at high concentration, the adsorption rate started to decrease for BC and MMT mainly due to the saturation of binding sites while that of MMT-BC was continuously increasing. The increased adsorption with increasing initial metal concentration can be attributed to two major factors, that is, (1) the possibility of collisions happening between Tl and ions of adsorbents and (2) a high distribution of Tl through adsorbents surface powered by increased driving force which decreases the transmission resistance.
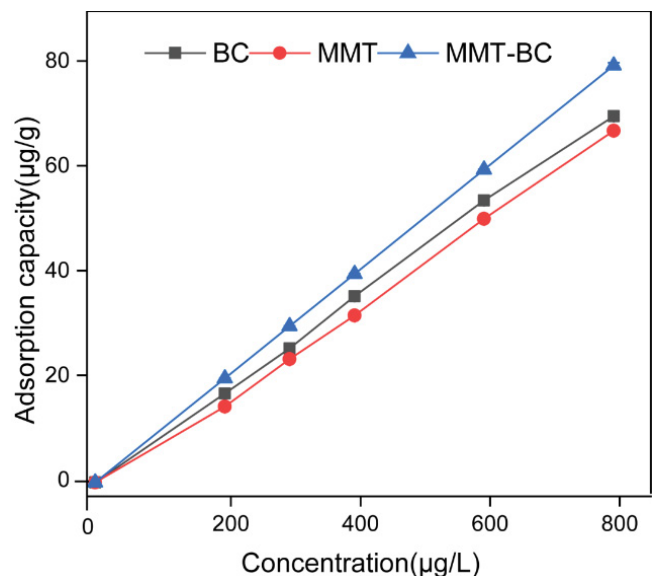
Fig. 3. Effect of initial concentration on Tl adsorption onto BC, MMT, and MMT-BC

Furthermore, the high adsorption capacity of MMT-BC than BC and MMT can be related to its high surface area, abundant negative charges, higher exchangeable Na and functional groups that increased the ion exchange between Tl and H^+/Na^+. In addition, it is due to the fact that MMT-BC combines the properties of BC and MMT which are also

good adsorbents to remove a high amount of Tl [44]. In contrast, the low adsorption capacity of MMT may be assigned to its regular shape and smoothness, low amount of exchangeable cations and low carbon content compared to other adsorbents in this study. More specifically, the Na ions in MMT were saturated and attached by van der Waals forces, making them non-exchangeable (Table S2). Here, two standard models were used to describe the isotherm adsorption process, that is, Langmuir model [48] and the Freundlich model [49]. Results showed that the adsorption fitted well Freundlich model as indicated by the correlation coefficients (R^2) (Fig. S10), and other fitting parameters are presented in (Table S4).

As the adsorbent's performance is controlled by various parameters including adsorption capacity, equilibrium time, regeneration, and cost, comparing adsorbents' performance under different adsorption conditions is difficult. Meanwhile, MMT-BC showed higher Tl adsorption capacity than bamboo biochar and montmorillonite used in this study under same conditions and in other's investigation [7]; also, it presented high adsorption percentage and high desorption percentage than the multi-walled carbon nanotubes [50]. Similarly, hypochlorite oxidation coupled with magnetite-based biochar, $MnFe_2O_4$-biochar composite and needle-shaped manganese oxide nanoparticle exhibited higher absorption capacity for Tl. However, they are expensively requiring careful pre-treatment, have low competition ability with cations and slow adsorption rate compared with MMT-BC, respectively [9,51,52].

3.2.3. Effect of time and adsorption kinetics

Tl removal was characterized by rapid adsorption in the early minutes of adsorption, followed by a gradual increase, and reached equilibrium in less than 1 h, as shown in Fig. 4. Within the first 10 min, the removal rate was above 90%, and by 30 min, it was around 100%. This is linked to the abundance of specific sites; that is, high surface area and porosity and high concentration gradient in the commencement [53]. As time goes on, the number of available active sites reduces, and the reduction in driving forces prolongs the equilibrium time; hence the adsorption process slows down. The results of this study
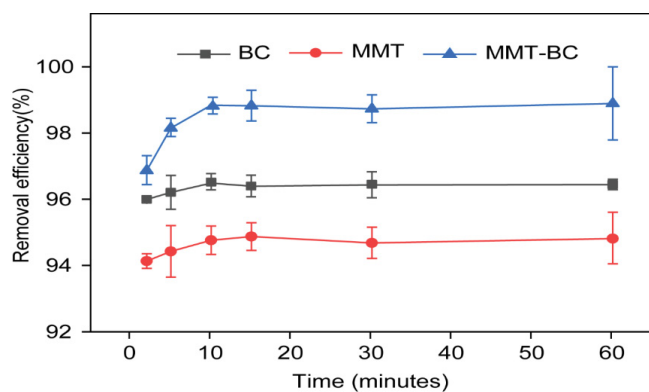
Fig. 4. Effect of time on Tl adsorption onto BC, MMT, and MMT-BC.

are comparable with the findings of other researches highlighting that Tl adsorption was observed to be fast in the beginning and, after reaching the equilibrium time, slowed down and remained almost constant [11].

The adsorption kinetics fitted well the pseudo-second-order model with R^2 above 0.9 (Fig. S11). In addition, the calculated adsorption q_e (µg/g) were close to the theoretical q_e values (Table S5). Accordingly, the best fit of pseudo-second-order model indicated that the adsorption of Tl was dominated by chemical forces such as ion exchange between Tl and Na^+/H^+, electrostatic attraction between positively charged Tl and negatively charged surface of adsorbents, and complexation reactions between Tl and oxygen-containing functional groups (OH) of the adsorbents [43].

3.2.4. Effect of ionic strength

The removal percentage of Tl decreased with increasing ionic concentration from 0.001 to 0.2 M (Fig. S9). However, the removal percentage of MMT-BC was still high (95.85%) when the concentration of $NaNO_3$ was 0.2 M. Tl adsorption on adsorbent binding sites was decreased due to competition for adsorption sites between Tl ions and Na^+ ions present in the background electrolyte ($NaNO_3$). It was significant because they have the same binding sites, and both of them are monovalent, which can increase their competition, thereby reducing Tl adsorption [54]. But also, the background electrolyte has reduced the negative charges of the adsorbents and enlarged the thickness of diffuse, which has resulted in the reduction of Tl adsorption [55].

3.2.5. Effect of co-existence with other heavy metals

In this study lead (Pb) and copper (Cu) have been used as model heavy metals because both are the principal metal ions found in waste water from mining plants as one of various sources of Tl contamination. An incompatible effect was found in competitive environments, suggesting that Cu^{2+} and Pb^{2+} are competing for the same adsorption sites with Tl, as shown in Fig. 5. At a low concentration of interfering heavy metals, the slight competition was observed for both metals, but with increasing the amount of interfering metal, the removal percentage was continuously decreasing as a sign of competition on the binding sites. Both Cu^{2+} and Pb^{2+} revealed lower competition on MMT-BC than on individual adsorbents. At equal concentration (100 µg/L) of Tl and Pb^{2+}, the removal percentage reduced from 99.75% to 97.79% and reduced from 99.75% to 93.66% at 500 µg/L (Fig. 5a). With Cu^{2+}, the removal percentage reduced from 99.75% to 96.11% at 100 µg/L, while at 500 µg/L it reduced from 99.75% to 95.1% (Fig. 5b). This might be due to on MMT-BC, Pb^{2+}/Cu^{2+} can bind with one or another adsorbent, thereby providing enough adsorption sites for Tl [56]. Comparing the variation of removal percentage with and without the interference of heavy metals (Pb^{2+} and Cu^{2+}), the results showed negligible change for Tl removal mainly due to the stoichiometric reactions between monovalent (Na^+) and divalent cations (Pb^{2+} and Cu^{2+}) during the ionic exchange is complicated.
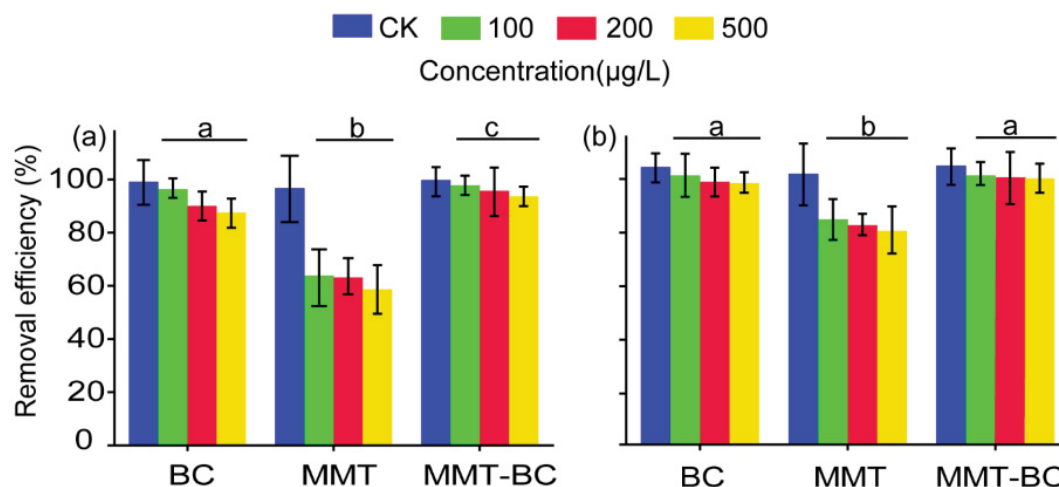
Fig. 5. Effect of co-existence with Pb^{2+} (a) and Cu^{2+} (b). Different letters indicate significant differences at $P < 0.05$ level.

3.2.6. Desorption

The recovery of Tl from the adsorbents was performed in acidic conditions using HNO_3 as elution agent and the results are presented in Fig. 6. The highest recovery of Tl was 89.4%, 83% and 98.9% for BC, MMT and MMT-BC. The obtained result complies with the reverse ion exchange reaction between Tl and H^+ in solution. It is clear that Tl can be simply desorbed and the adsorbents can be restored at a high degree which increases its usage in removing further Tl in other cycles and making the removal process more economical. Regeneration study should be done in order to know the adsorption capacity of the adsorbents after numerous cycles.

3.2.7. Adsorption mechanism

As summarized, the well-fitting of the Freundlich model during isotherm studies highlighted that Tl adsorption onto MMT-BC belongs to the heterogeneous surface and no formation of a monolayer. Similarly, the well-fitted pseudo-second-order model from kinetic studies confirmed that chemical forces dominated Tl adsorptions through ion exchange, electrostatic attraction and complexation. Specifically, the spectrum from EDS characterization discloses the formation of new peaks position on the image after adsorption. It is attributed to the accumulation of Tl on MMT-BC through ion exchange between cations and Tl and complexation between Tl and oxygen – containing functional groups [57].

FTIR and XPS results showed –OH groups on MMT-BC, which could stimulate the ion exchange between Tl and H^+ and complexation on oxygen-containing functional groups. After adsorption, the reduction in spectrum peak position observed on FTIR as a result of the accumulation of Tl through complexation or ion exchange and electrostatic attraction [43]. Additionally, the results from exchangeable cations analysis revealed the presence of exchangeable cations in MMT-BC, which encouraged their exchange with Tl. Again, the increase of adsorption percentage with increasing pH indicates the possibility of electrostatic attraction between positively charged Tl and the surface of the
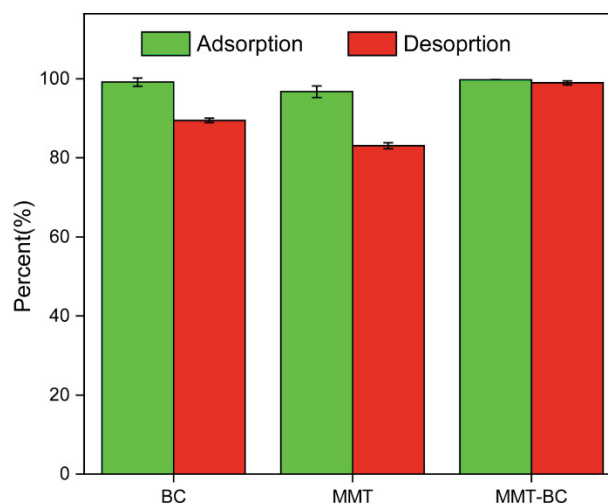
Fig. 6. Desorption studies of Tl from BC, MMT and MMT-BC.

adsorbents, which is negatively charged. Moreover, besides its high surface area, porosity, and more oxygen-containing functional groups, the high amount of exchangeable Na in MMT-BC could explain its high removal efficiency than BC and MMT. The study of [58] reported Tl is mainly adsorbed by ion exchange between Tl and Na^+ due to both Tl and Na^+ are monovalent cations, and their exchange is relatively easy.

During MMT-BC preparation, MMT increased the oxygen containing functional groups [59], which have promoted the formation of new pores and increased reactive sites on the surface. From the findings of this study, we consider that the accumulation of Tl ions onto MMT-BC through its exchange with Na ions, electrostatic attraction and complexation with the hydroxyl, carboxyl and silanol functional groups are the best description for Tl adsorption mechanism (Fig. 7).

3.3. Environmental implications

Tl contamination has increased primarily in developed countries, jeopardizing human health and the ecosystem
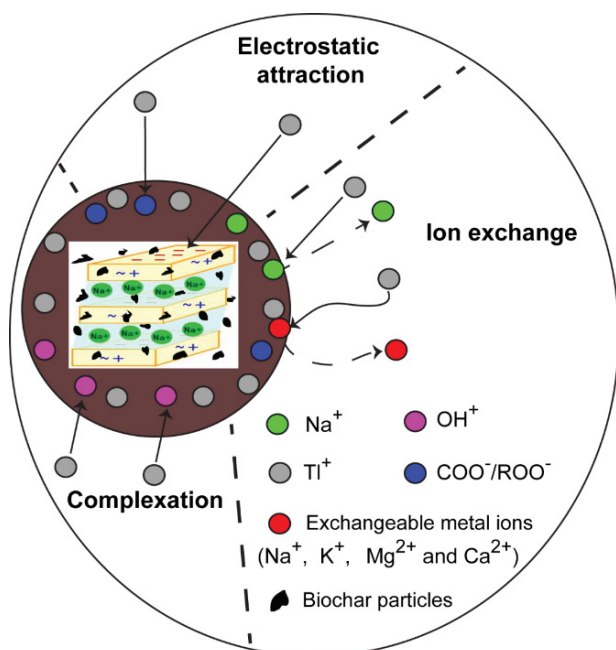
Fig. 7. Potential adsorption mechanism of Tl onto MMT-BC.

in general [11]. The current study has developed a montmorillonite biochar composite (MMT-BC) and tested its potential Tl remediation for the first time. MMT-BC showed a quick and high removal rate towards Tl under different environmental conditions from acidic to alkaline environments. MMT-BC showed high Tl removal in co-existence with other heavy metals and under high ionic strength. Additionally, the high desorption percentage as displayed, confirmed that the adsorbents were almost fully recovered which increases its usage in removing further Tl in other cycles and making the removal process more economical. Thus, in addition to the low cost of BC and MMT as precursors of MMT-BC, and environmental friendliness, the factors mentioned above can suffice for recommending MMT-BC to be used in remediation of Tl contaminated aqueous environments and agricultural soils. Accordingly, its potential application would be favored to improve environmental health status due to Tl's higher adsorption capacity. However, further investigations are still required to assess its regeneration capacity.

4. Conclusion

A montmorillonite biochar composite (MMT-BC) from bamboo-derived biochar (BC) and montmorillonite (MMT) was successfully produced and used for the first time to remove Tl in aqueous environments through its adsorption. As observed, the MMT-BC displayed porosity, roughness and more functional groups on its surface. Tl was removed from pH 2 to 10 with more than 80% removal at pH 2 and around 100% at pH 10. The kinetic adsorption data fitted the pseudo-second-order model with a correlation coefficient ($R^2 > 0.9$). The equilibrium was attained within 10 min, indicating that chemisorption predominated through ion exchange, electrostatic attraction and complexation. The isotherm studies fit the Freundlich model well, and the highest adsorption capacity of 79.7 µg/g was obtained using MMT-BC when the initial concentration was 800 µg/L. MMT-BC presented high selectivity for Tl in competition with other heavy metals. In addition, the desorption percentage was around 100%. This study showed how MMT-BC is environmentally friendly and can remove Tl in aqueous environments and can be used in remediation of agricultural soils contaminated by Tl to improve their health conditions, including carbon sequestration.

Declaration of interests

On behalf of all authors, the corresponding author states that there is no conflict of interest.

Acknowledgement

References

[1] M. Czikkely, E. Neubauer, I. Fekete, P. Ymeri, C. Fogarassy, Review of heavy metal adsorption processes by several organic matters from wastewaters, Water, 10 (2018) 1377, doi: 10.3390/w10101377.

[2] A. Müller, H. Österlund, J. Marsalek, M. Viklander, The pollution conveyed by urban runoff: a review of sources, Sci. Total Environ., 709 (2020) 136125, doi: 10.1016/j.scitotenv.2019.136125.

[3] A. Selvi, A. Rajasekar, J. Theerthagiri, A. Ananthaselvam, K. Sathishkumar, J. Madhavan, P.K.S.M. Rahman, Integrated remediation processes toward heavy metal removal/recovery from various environments-a review, Front. Environ. Sci., 7 (2019), doi: 10.3389/fenvs.2019.00066.

[4] K.H. Vardhan, P.S. Kumar, R.C. Panda, A review on heavy metal pollution, toxicity and remedial measures: Current trends and future perspectives, J. Mol. Liq., 290 (2019) 111197, doi: 10.1016/j.molliq.2019.111197.

[5] H. Li, Y. Chen, J. Long, D. Jiang, J. Liu, S. Li, J. Qi, P. Zhang, J. Wang, J. Gong, Q. Wu, D. Chen, Simultaneous removal of thallium and chloride from a highly saline industrial wastewater using modified anion exchange resins, J. Hazard. Mater., 333 (2017) 179–185.

[6] N. Belzile, Y. Chen, Thallium in the environment: a critical review focused on natural waters, soils, sediments and airborne particles, Appl. Geochem., (2017), doi: 10.1016/j.apgeochem.2017.06.013.

[7] A. Kayiranga, Z. Luo, J.C. Ndayishimiye, F. Nkinahamira, E. Cyubahiro, T. Habumugisha, C. Yan, J. Guo, Z. Zhen, A. Tuyishimire, H.D. Izabayo, Insights into thallium adsorption onto the soil, bamboo-derived biochar, and biochar amended soil in Pomelo orchard, Biochar, 3 (2021), doi: 10.1007/s42773-021-00095-1.

[8] H. Li, J. Xiong, T. Xiao, J. Long, Q. Wang, K. Li, X. Liu, G. Zhang, H. Zhang, Biochar derived from watermelon rinds as regenerable adsorbent for efficient removal of thallium(I) from wastewater, Process Saf. Environ. Prot., 127 (2019) 257–266.

[9] H. Li, J. Xiong, G. Zhang, A. Liang, J. Long, T. Xiao, Y. Chen, P. Zhang, D. Liao, L. Lin, H. Zhang, Enhanced thallium(I) removal from wastewater using hypochlorite oxidation coupled

with magnetite-based biochar adsorption, Sci. Total Environ., 698 (2020) 134166, doi: 10.1016/j.scitotenv.2019.134166.

[10] J. Liu, N. Li, W. Zhang, X. Wei, D.C.W. Tsang, Y. Sun, X. Luo, W. Zheng, J. Wang, G. Xu, L. Hou, Y. Chen, Y. Feng, Thallium contamination in farmlands and common vegetables in a pyrite mining city and potential health risks, Environ. Pollut., 248 (2019) 906–915.

[11] J. Liu, S. Ren, J. Cao, D.C.W. Tsang, J. Beiyuan, Y. Peng, F. Fang, J. She, M. Yin, N. Shen, J. Wang, Highly efficient removal of thallium in wastewater by MnFe$_2$O$_4$-biochar composite, J. Hazard. Mater., 401 (2021) 123311, doi: 10.1016/j.jhazmat.2020.123311.

[12] W. Huang, B. Song, J. Liang, Q. Niu, G. Zeng, M. Shen, J. Deng, Y. Luo, X. Wen, Y. Zhang, Microplastics and associated contaminants in the aquatic environment: a review on their ecotoxicological effects, trophic transfer, and potential impacts to human health, J. Hazard. Mater., 405 (2021) 124187, doi: 10.1016/j.jhazmat.2020.124187.

[13] H. Li, Y. Chen, J. Long, X. Li, D. Jiang, P. Zhang, J. Qi, X. Huang, J. Liu, R. Xu, J. Gong, Removal of thallium from aqueous solutions using Fe-Mn binary oxides, J. Hazard. Mater., 338 (2017) 296–305.

[14] X. Yang, L. Liu, W. Tan, C. Liu, Z. Dang, G. Qiu, Remediation of heavy metal contaminated soils by organic acid extraction and electrochemical adsorption, Environ. Pollut., 264 (2020) 114745, doi: 10.1016/j.envpol.2020.114745.

[15] T. Bohli, A. Ouederni, I. Villaescusa, Simultaneous adsorption behavior of heavy metals onto microporous olive stones activated carbon: analysis of metal interactions, Euro-Mediterr. J. Environ. Integr., 2 (2017), doi: 10.1007/s41207-017-0030-0.

[16] B.J. Ni, Q.S. Huang, C. Wang, T.Y. Ni, J. Sun, W. Wei, Competitive adsorption of heavy metals in aqueous solution onto biochar derived from anaerobically digested sludge, Chemosphere, 219 (2019) 351–357.

[17] H. Xu, Y. Luo, P. Wang, J. Zhu, Z. Yang, Z. Liu, Removal of thallium in water/wastewater: a review, Water Res., 165 (2019) 114981, doi: 10.1016/j.watres.2019.114981.

[18] F. Nkinahamira, A. Alsbaiee, Q. Zeng, Y. Li, Y. Zhang, M. Feng, C.P. Yu, Q. Sun, Selective and fast recovery of rare earth elements from industrial wastewater by porous β-cyclodextrin and magnetic β-cyclodextrin polymers, Water Res., 181 (2020) 115857, doi: 10.1016/j.watres.2020.115857.

[19] L. Beesley, E. Moreno-Jiménez, J.L. Gomez-Eyles, E. Harris, B. Robinson, T. Sizmur, A review of biochars' potential role in the remediation, revegetation and restoration of contaminated soils, Environ. Pollut., 159 (2011) 3269–3282.

[20] L. Wang, Y.S. Ok, D.C.W. Tsang, D.S. Alessi, J. Rinklebe, H. Wang, O. Mašek, R. Hou, D. O'Connor, D. Hou, New trends in biochar pyrolysis and modification strategies: feedstock, pyrolysis conditions, sustainability concerns and implications for soil amendment, Soil Use Manage., (2020) 1–29, doi: 10.1111/sum.12592.

[21] E.F. Zama, B.J. Reid, H.P.H. Arp, G.X. Sun, H.Y. Yuan, Y.G. Zhu, Advances in research on the use of biochar in soil for remediation: a review, J. Soils Sedim., 18 (2018) 2433–2450.

[22] Z. Luo, C.A. Secondary, C. Author, Z. Luo, A. Kayiranga, E. Uwiringiyimana, Z. Qinghua, C. Yan, J. Guo, Biochar thallium contamination in agricultural soils and associated potential remediation by utilization of biochar, (n.d.).

[23] Y. Hou, G. Huang, J. Li, Q. Yang, S. Huang, J. Cai, Hydrothermal conversion of bamboo shoot shell to biochar: preliminary studies of adsorption equilibrium and kinetics for rhodamine B removal, J. Anal. Appl. Pyrolysis, 143 (2019) 104694, doi: 10.1016/j.jaap.2019.104694.

[24] N.M. Alandis, W. Mekhamer, O. Aldayel, J.A.A. Hefne, M. Alam, Adsorptive applications of montmorillonite clay for the removal of Ag(I) and Cu(II) from aqueous medium, J. Chem., 2019 (2019), doi: 10.1155/2019/7129014.

[25] G. Yang, Y. Jiang, X. Yang, Y. Xu, S. Miao, F. Li, The interaction of cellulose and montmorillonite in a hydrothermal process, J. Sol-Gel Sci. Technol., 82 (2017) 846–854.

[26] B. Chu, Y. Amano, M. Machida, Preparation of bamboo-based oxidized biochar for simultaneous removal of Cd(II) and

Cr(VI) from aqueous solutions, Desal. Water Treat., 168 (2019) 269–281.

[27] S. Gu, X. Kang, L. Wang, E. Lichtfouse, C. Wang, Clay mineral adsorbents for heavy metal removal from wastewater: a review, Environ. Chem. Lett., 17 (2019) 629–654.

[28] C. Zhang, N. Zhang, Z. Xiao, Z. Li, D. Zhang, Characterization of biochars derived from different materials and their effects on microbial dechlorination of pentachlorophenol in a consortium, RSC Adv., 9 (2019) 917–923.

[29] Z. Mahdi, Q.J. Yu, A. El, Removal of lead(II) from aqueous solution using date seed – derived biochar: batch and column studies, Appl. Water Sci., (2018), doi: 10.1007/s13201-018-0829-0.

[30] L. Chen, X.L. Chen, C.H. Zhou, H.M. Yang, S.F. Ji, D.S. Tong, Z.K. Zhong, W.H. Yu, M.Q. Chu, Environmental-friendly montmorillonite-biochar composites: facile production and tunable adsorption-release of ammonium and phosphate, J. Cleaner Prod., 156 (2017) 648–659.

[31] J. Zhang, M. Lu, J. Wan, Y. Sun, H. Lan, X. Deng, Effects of pH, dissolved humic acid and Cu^{2+} on the adsorption of norfloxacin on montmorillonite-biochar composite derived from wheat straw, Biochem. Eng. J., 130 (2018) 104–112.

[32] B.O. Otunola, O.O. Ololade, A review on the application of clay minerals as heavy metal adsorbents for remediation purposes, Environ. Technol. Innov., 18 (2020) 100692, doi: 10.1016/j.eti.2020.100692.

[33] M. Thommes, K. Kaneko, A.V. Neimark, J.P. Olivier, F. Rodriguez-Reinoso, J. Rouquerol, K.S.W. Sing, Physisorption of gases, with special reference to the evaluation of surface area and pore size distribution (IUPAC Technical Report), Pure Appl. Chem., 87 (2015) 1051–1069.

[34] E. Viglašová, M. Galamboš, Z. Danková, L. Krivosudský, C.L. Lengauer, R. Hood-Nowotny, G. Soja, A. Rompel, M. Matík, J. Briančin, Production, characterization and adsorption studies of bamboo-based biochar/montmorillonite composite for nitrate removal, Waste Manage., 79 (2018) 385–394.

[35] K.S.D. Premarathna, A.U. Rajapaksha, B. Sarkar, E.E. Kwon, A. Bhatnagar, Y.S. Ok, M. Vithanage, Biochar-based engineered composites for sorptive decontamination of water: a review, Chem. Eng. J., 372 (2019) 536–550.

[36] Y. Yao, B. Gao, J. Fang, M. Zhang, H. Chen, Y. Zhou, A.E. Creamer, Y. Sun, L. Yang, Characterization and environmental applications of clay-biochar composites, Chem. Eng. J., 242 (2014) 136–143.

[37] J. Song, S. Zhang, G. Li, Q. Du, F. Yang, Preparation of montmorillonite modified biochar with various temperatures and their mechanism for Zn ion removal, J. Hazard. Mater., 391 (2020) 121692, doi: 10.1016/j.jhazmat.2019.121692.

[38] B. Priyadarshini, P.P. Rath, S.S. Behera, S.R. Panda, T.R. Sahoo, P.K. Parhi, Kinetics, Thermodynamics and Isotherm studies on adsorption of Eriochrome Black-T from aqueous solution using rutile TiO$_2$, IOP Conf. Ser.: Mater. Sci. Eng., 310 (2018), doi: 10.1088/1757-899X/310/1/012051.

[39] D. Chen, K. Cen, X. Cao, F. Chen, J. Zhang, J. Zhou, Insight into a new phenolic-leaching pretreatment on bamboo pyrolysis: release characteristics of pyrolytic volatiles, upgradation of three phase products, migration of elements, and energy yield, Renewable Sustainable Energy Rev., 136 (2021) 110444, doi: 10.1016/j.rser.2020.110444.

[40] B.A. Fil, C. Özmetin, M. Korkmaz, Characterization and electrokinetic properties of montmorillonite, Bulg. Chem. Commun., 46 (2014) 258–263.

[41] E.W. Maina, H.J. Wanyika, A.N. Gacanja, Instrumental characterization of montmorillonite clay by FT-IR and XRD from J.K.U.A.T farm, in the Republic of Kenya, Chem. Mater. Res., 7 (2015) 43–49.

[42] J. Zhang, M. Lu, J. Wan, Y. Sun, H. Lan, X. Deng, Effects of pH, dissolved humic acid and Cu^{2+} on the adsorption of norfloxacin on montmorillonite-biochar composite derived from wheat straw, Biochem. Eng. J., 130 (2018) 104–112.

[43] H. Li, X. Li, Y. Chen, J. Long, G. Zhang, T. Xiao, P. Zhang, C. Li, L. Zhuang, W. Huang, Removal and recovery of thallium from aqueous solutions via a magnetite-mediated reversible

adsorption–desorption process, J. Cleaner Prod., 199 (2018) 705–715.

[44] G. Liang, Z. Wang, X. Yang, T. Qin, X. Xie, J. Zhao, S. Li, Efficient removal of oxytetracycline from aqueous solution using magnetic montmorillonite-biochar composite prepared by one step pyrolysis, Sci. Total Environ., 695 (2019) 133800, doi: 10.1016/j.scitotenv.2019.133800.

[45] Yuri, G.A. Ayoko, R.L. Frost, Characterisation of organoclays and adsorption of p-nitrophenol: Environmental application, J. Colloid Interface Sci., 360 (2011) 440–456.

[46] B. Ruiz-Camacho, J.A. Palafox-Segoviano, P.J. Pérez-Díaz, A. Medina-Ramírez, Synthesis of supported Pt nanoparticles by sonication for ORR: effect of the graphene oxide-carbon composite, Int. J. Hydrogen Energy, 46 (2021) 26027–26039.

[47] S. Pletincx, L. Trotochaud, L.L. Fockaert, J.M.C. Mol, A.R. Head, O. Karslloğlu, H. Bluhm, H. Terryn, T. Hauffman, In situ characterization of the initial effect of water on molecular interactions at the interface of organic/inorganic hybrid systems, Sci. Rep., 7 (2017) 3–10.

[48] G. Vilardi, T. Mpouras, D. Dermatas, N. Verdone, A. Polydera, L. Di Palma, Nanomaterials application for heavy metals recovery from polluted water: the combination of nano zero-valent iron and carbon nanotubes. Competitive adsorption non-linear modeling, Chemosphere, 201 (2018) 716–729.

[49] H.A. Alalwan, M.A. Kadhom, A.H. Alminshid, Removal of heavy metals from wastewater using agricultural byproducts, J. Water Supply Res. Technol. AQUA, 69 (2020) 99–112.

[50] Y. Pu, X. Yang, H. Zheng, D. Wang, Y. Su, J. He, Adsorption and desorption of thallium(I) on multiwalled carbon nanotubes, Chem. Eng. J., 219 (2013) 403–410.

[51] J. Liu, S. Ren, J. Cao, D.C.W. Tsang, J. Beiyuan, Y. Peng, F. Fang, J. She, M. Yin, N. Shen, J. Wang, Highly efficient removal of thallium in wastewater by $MnFe_2O_4$-biochar composite, J. Hazard. Mater., 401 (2021) 123311, doi: 10.1016/j.jhazmat.2020.123311.

[52] Z. Ren, W. Wu, L. Yu, Y. Yu, Hydrothermal synthesis of needle-shaped manganese oxide nanoparticle for superior adsorption of thallium(I): characterization, performance, and mechanism study, Environ. Sci. Pollut. Res. Int., 26 (2019) 36776–36785.

[53] S.Q. Memon, N. Memon, A.R. Solangi, J. ur R. Memon, Sawdust: a green and economical sorbent for thallium removal, Chem. Eng. J., 140 (2008) 235–240.

[54] L.A. Martin, A. Wissocq, M.F. Benedetti, C. Latrille, Thallium (Tl) sorption onto illite and smectite: Implications for Tl mobility in the environment, Geochim. Cosmochim. Acta, 230 (2018) 1–16.

[55] H.M. Deng, Y.H. Chen, H.H. Wu, T. Liu, Y.L. Wang, G.Y. Wu, H.P. Ye, Adsorption of Tl(I) on Na–montmorillonite and kaolinite from aqueous solutions, Environ. Earth Sci., 75 (2016), doi: 10.1007/s12665-016-5570-0.

[56] H. Du, W. Chen, P. Cai, X. Rong, X. Feng, Q. Huang, Competitive adsorption of Pb and Cd on bacteria–montmorillonite composite, Environ. Pollut., 218 (2016) 168–175.

[57] J. Tang, W. Wu, L. Yu, X. Fan, G. Liu, Y. Yu, Study on adsorption properties and mechanism of thallium onto titanium iron magnetic adsorbent, Sci. Total Environ., 694 (2019) 133625, doi: 10.1016/j.scitotenv.2019.133625.

[58] W. Liu, P. Zhang, A.G.L. Borthwick, H. Chen, J. Ni, Adsorption mechanisms of thallium(I) and thallium(III) by titanate nanotubes: ion-exchange and co-precipitation, J. Colloid Interface Sci., 423 (2014) 67–75.

[59] N. Zhou, Y. Wang, L. Huang, J. Yu, H. Chen, J. Tang, F. Xu, X. Lu, M e. Zhong, Z. Zhou, In situ modification provided by a novel wet pyrolysis system to enhance surface properties of biochar for lead immobilization, Colloids Surf., A, 570 (2019) 39–47.

Supplementary information

S1. Effect of adsorbent dosage

Generally, the removal efficiency increased as increasing the dose of adsorbents (Fig. S5). Thallium (Tl) (I) removal efficiency was greater than 90% at an adsorbent dosage of 2 g/L for all the adsorbents. Similar results were obtained when removing Tl using magnetic Prussian Blue derivative [S1] and Na–montmorillonite and kaolinite [S2] from aqueous solutions. At low adsorbent dosage, the only limiting factor is the availability of adsorbent active sites on the surface of the adsorbent [S3]. Therefore, the elevated removal rate at higher adsorbent dosage can be ascribed to the availability of adsorption sites on the adsorbent surface [S4]. Nevertheless, the aggregation and overlapping of particles at high adsorbent dosage resulted in the reduction of adsorption sites on the surface; consequently the adsorption capacity decreases [S5]. Since the results found using 40 g/L is comparable with that found with 8 g/L, which is 5 times higher there is no need to use a high amount of adsorbent to adsorb Tl in this study. Thus, considering the removal efficiency and

economical point of view, the adsorbent dose of 10 g/L was chosen for the following adsorption experiments.

S2. Effect of rotation speed

The rotation speed plays a critical role in the solute-solvent mass transfer mechanism influencing the external boundary layer and circulation of the solute in the bulk solution. The effect of rotation speed was studied in a range of 50 to 400 rpm. As illustrated in Fig. S6, the adsorption percentage was higher than 80% at a rotation speed of 50 rpm.

Table S2
Exchangeable cations distribution in BC, MMT and MMT-BC (cmol/Kg)

Adsorbents	Ca	K	Mg	Na
BC	30.65	14.5	13.39	2.58
MMT	11.03	4.8	42.33	Saturated
MMT-BC	4.56	2.5	5.79	20.83

Table S1
Elemental composition (%) of the samples by CNS

Samples/Elements	N	C	S	O	(O+N+S)	O/C	(O+N+S)/C
BC	2.48	22.37	0.3	74.83	77.621	3.343	22.379
MMT	0.04	0.28	0.05	99.61	99.714	348.311	348.65
MMT-BC	0.33	3.65	0.08	95.93	96.35	26.27	26.382
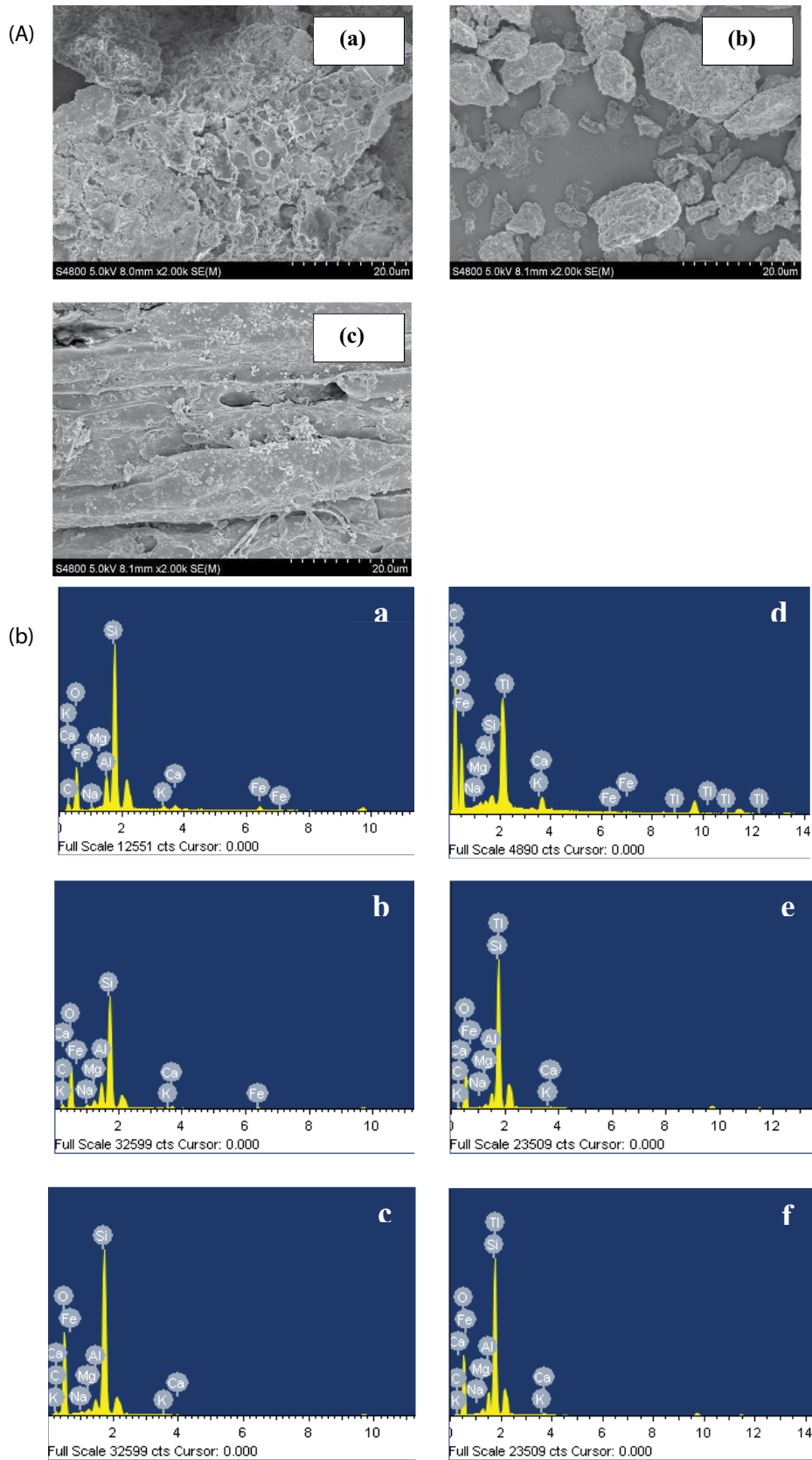
Fig. S1. (A) SEM images of BC (a), MMT (b) and MMT-BC (c). (B) EDS images of BC, MMT and MMT-BC (a–c), respectively before adsorption and (d–f) after adsorption.

Table S3
SSA, pore size and pore volume of BC, MMT and MMT-BC

Adsorbent/property	Specific surface area (m²/g)	Pore volume (cm³/g)	Pore size (nm)
BC	7.76	0.02	10.98
MMT	47.22	0.10	8.95
MMT-BC	27.10	0.06	9.42

Table S4
Isotherm parameters for adsorption of Tl on BC, MMT and MMT-BC

Adsorbents	Freundlich model		
Parameters	n	K_F (mg/g (L/mg)$^{1/n}$)	R^2
BC	0.84	3.04	0.9097
MMT	0.55	11.97	0.9684
MMT-BC	0.6	2.77	0.9487

Table S5
Kinetic parameters for adsorption of Tl on BC, MMT, and MMT-BC

Adsorbents	Pseudo-second-order model		
	k_2 (min^{-1})	$q_{e,cal}$ (µg/g)	R^2
BC	0.40	9.77	0.98
MMT	0.15	9.92	0.94
MMT-BC	0.47	10.01	0.98

The highest adsorption of thallium into biochar (BC), and montmorillonite biochar (MMT-BC) reached 98.8% and 99.9% respectively at a rotation speed of 300 rpm while for montmorillonite (MMT) the highest adsorption percentage of 95.6% was obtained at 400 rpm.

The adsorption was increasing with the rotation speed because the increased turbulence and reduction of thickness of the liquid enhanced the diffusion rate of Tl into the liquid boundary layer covering the adsorbents surface [S6]. However, at a rotation speed greater than 200 rpm, the variation in adsorption rate is negligible and tends to shrink suggesting that the film thickness has little effect when the rotation speed is above 300 rpm. The low adsorption at low rotation speed is due to low mass transfer of thallium

1–SiO$_2$ 2–CaCO$_3$ 3–(Na,Ca)Al(Si,Al)$_3$O$_8$
4–Mg$_{1.40}$Fe$_{0.66}$Al$_{3.96}$Si$_{5.04}$O$_{18}$ 5–Fe$_3$O$_4$
6–K$_{0.69}$(Fe$_{0.02}$Mg$_{1.98}$)(Si$_{10.4}$Al$_{1.6}$)(Fe$_{0.24}$Al$_{2.76}$)O$_{30}$

1–Si O$_2$ 2–C 3–Na-Ca-Al-Si$_4$O$_{10}$-O
4–Na$_{0.45}$Ca$_{0.55}$Al$_{1.55}$Si$_{2.45}$O$_8$

1–SiO$_2$ 2–Na$_{92}$(Si$_{100}$Al$_{92}$O$_{384}$)
3–(Na$_{0.84}$Ca$_{0.16}$)Al$_{1.16}$Si$_{2.84}$O$_8$ 4–Ca$_{0.07}$ Al$_{0.16}$Si$_{0.84}$O$_2$
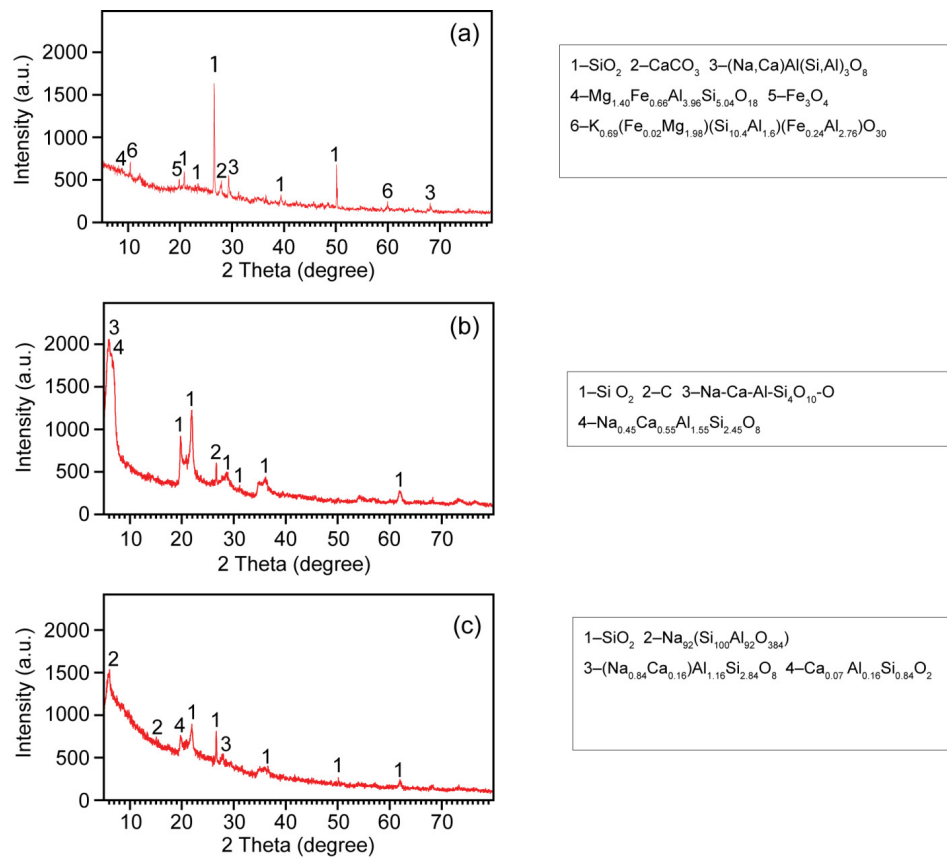
Fig. S2. XRD images of BC (a), MMT (b), and MMT-BC (c).
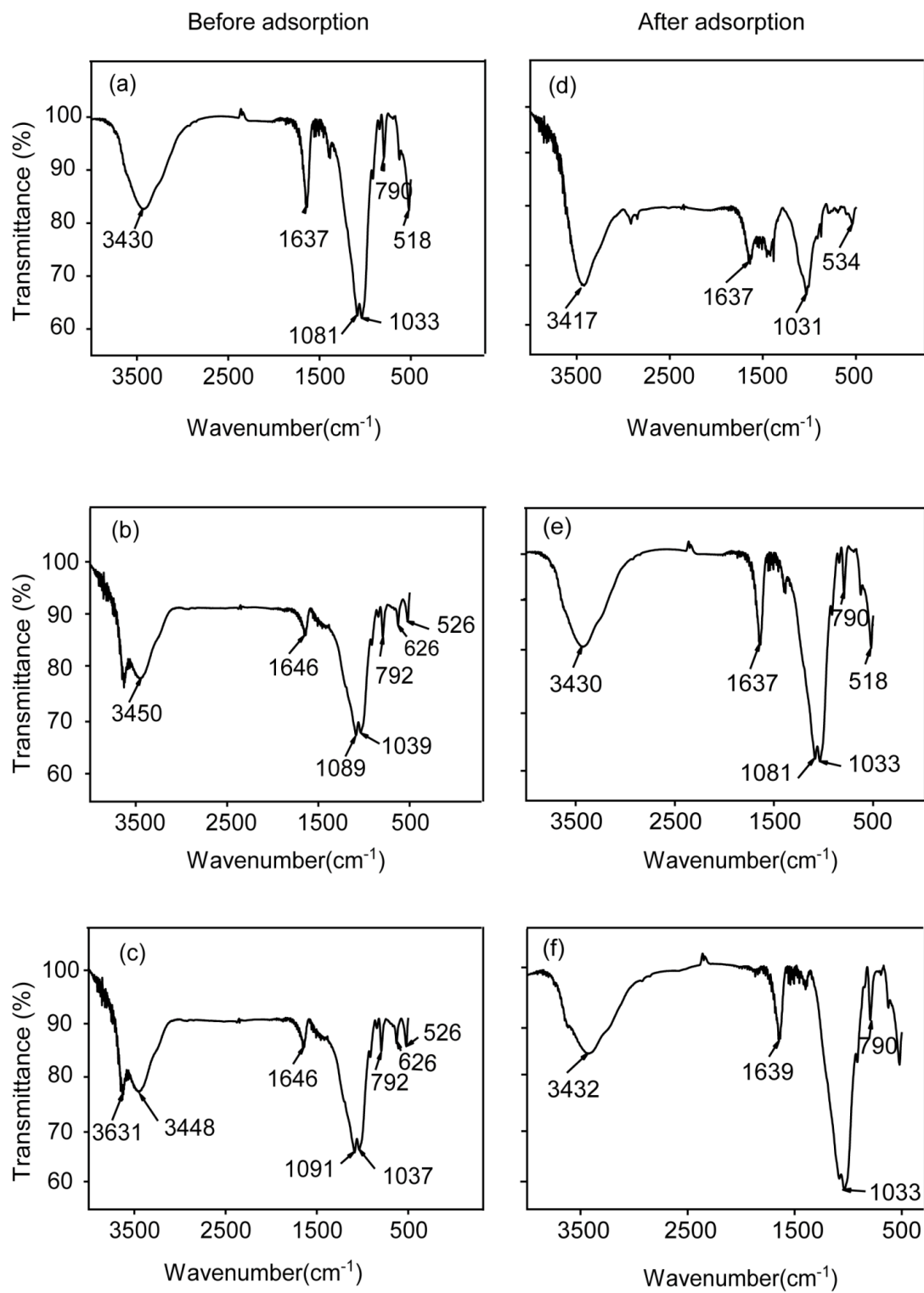
Fig. S3. FTIR images of BC (a), MMT (b), and MMT-BC (c) before adsorption and BC (d), MMT (e), and MMT-BC (f) after adsorption.
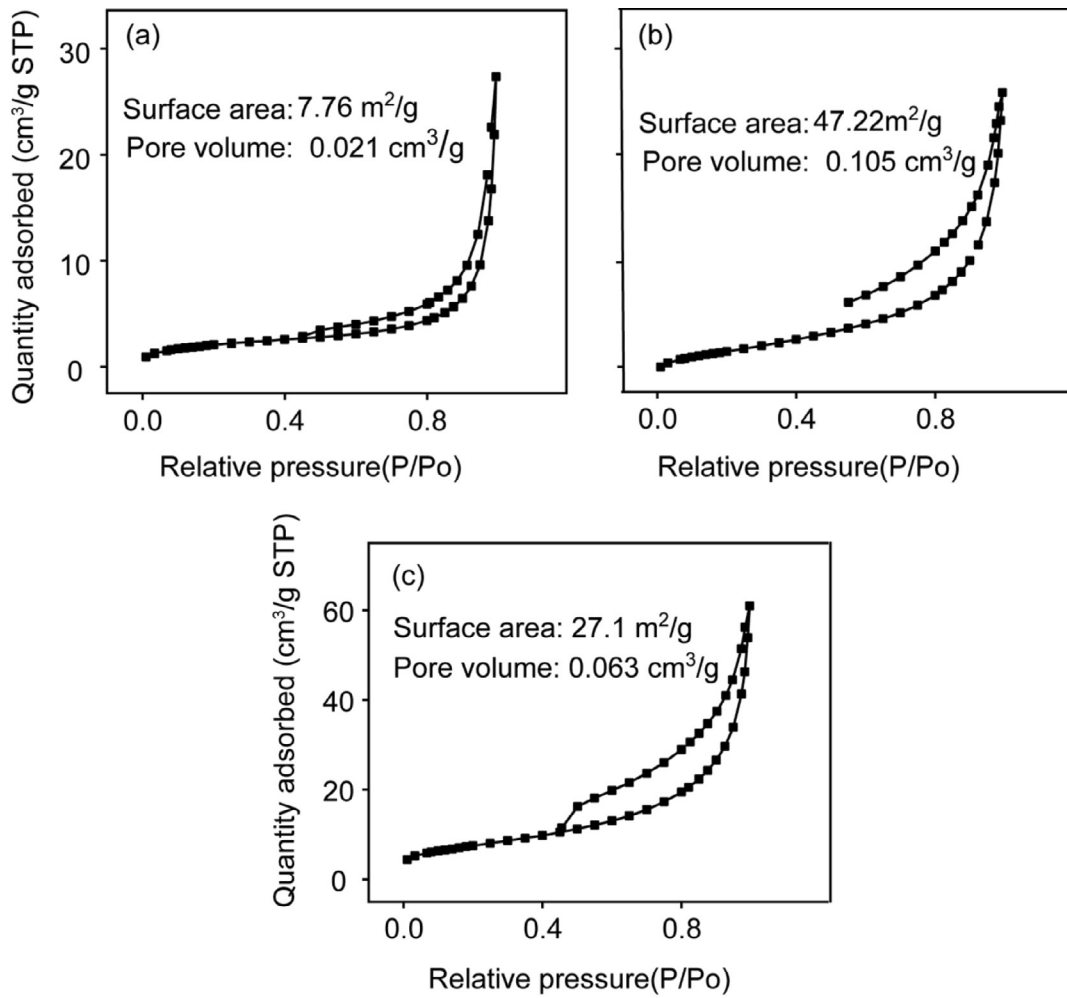
Fig. S4. Nitrogen adsorption–desorption isotherms at 77 K for BC (a), MMT (b) and MMT-BC (c).
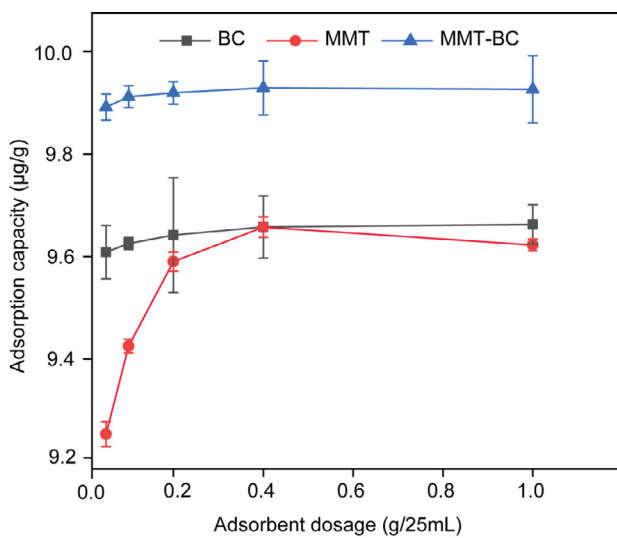
Fig. S5. Effect of adsorbent dosage (g/25 mL) on Tl adsorption onto BC, MMT, and MMT-BC.
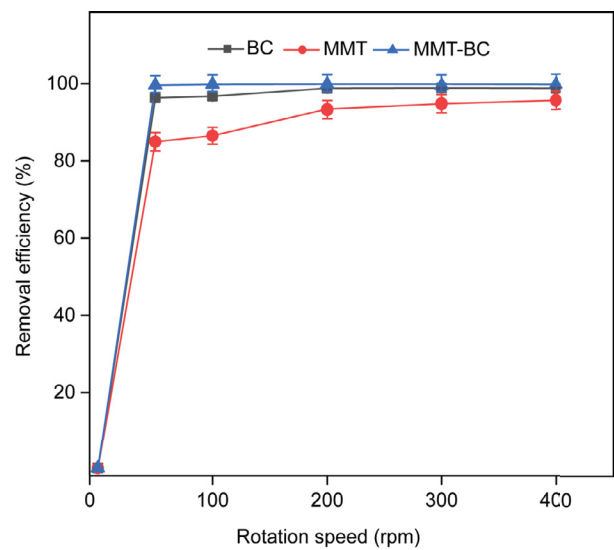
Fig. S6. Effect of agitation speed on Tl adsorption onto BC, MMT, and MMT-BC.
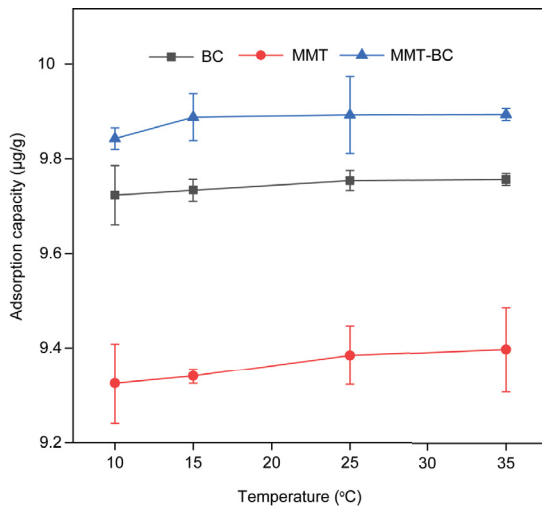
Fig. S7. Effect of temperature on Tl adsorption onto BC, MMT, and MMT-BC.
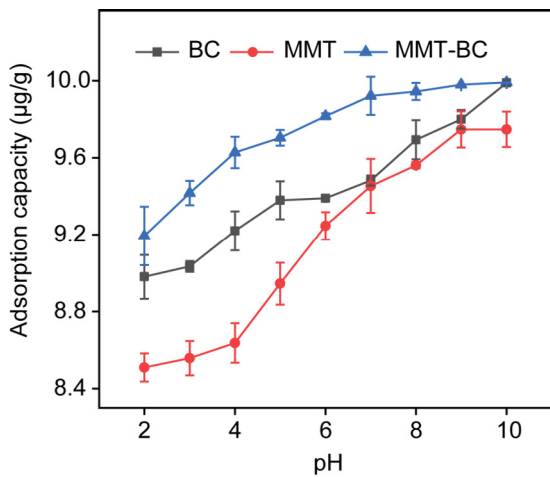
Fig. S8. Effect of pH on Tl adsorption onto BC, MMT, and MMT-BC.
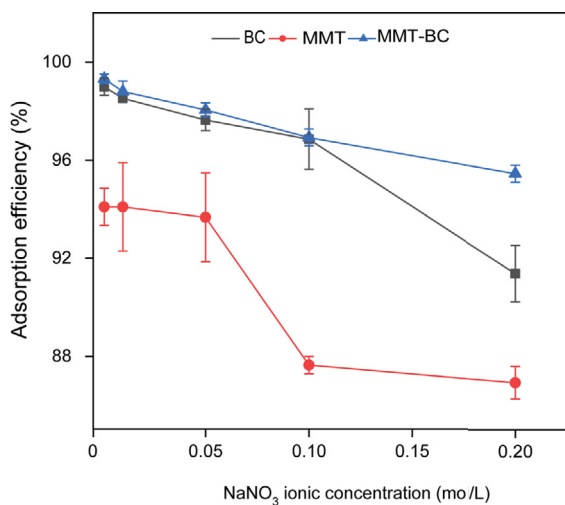
Fig. S9. Effect of ionic strength (mol/L) on Tl adsorption onto BC, MMT, and MMT-BC.
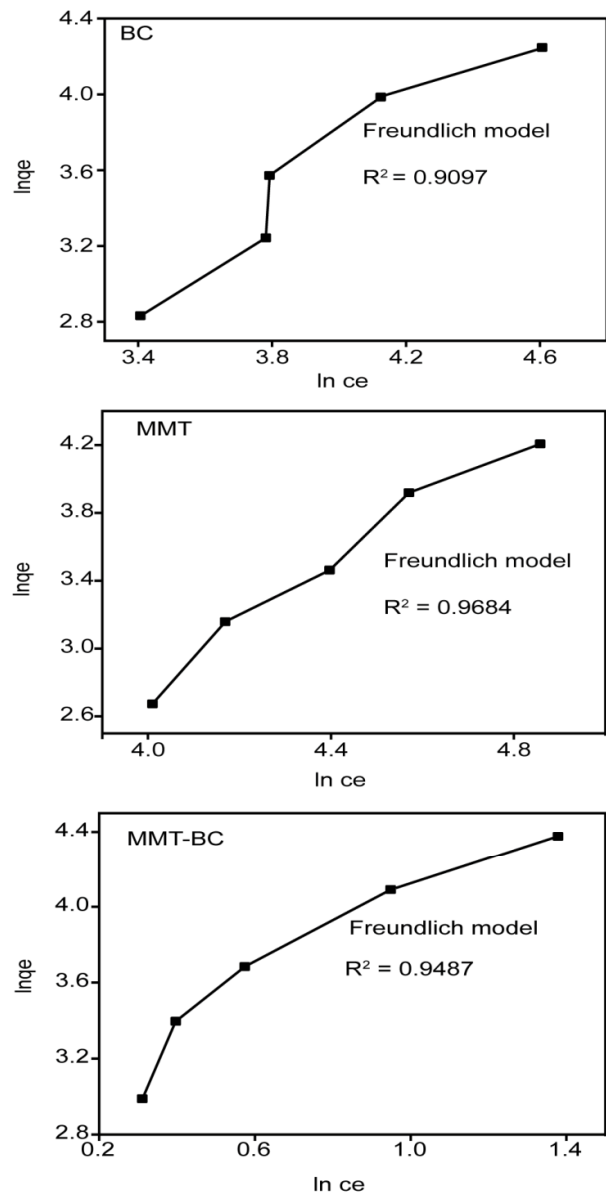
Fig. S10. Freundlich isotherms of adsorption.

into the materials' surface from inadequate dispersion but also higher rotation speed may cause the collision between Tl and adsorbents particles which lead to desorption when the equilibrium is reached [S7] affecting the kinetics and the overall adsorption capacity [S8]. Therefore, 200 rpm has been selected to conduct other experiments.

S3. Effect of solution temperature

The solution temperature plays a critical role when studying the adsorption process. Fig. S7 displays the change in Tl removal with temperature of the solution. As it is shown on the figure, the removal percentage was increasing with temperature and the peak values were observed around 25°C for all the adsorbents. The increase of adsorption with temperature is due to high temperature reduces the stickiness of the solution and
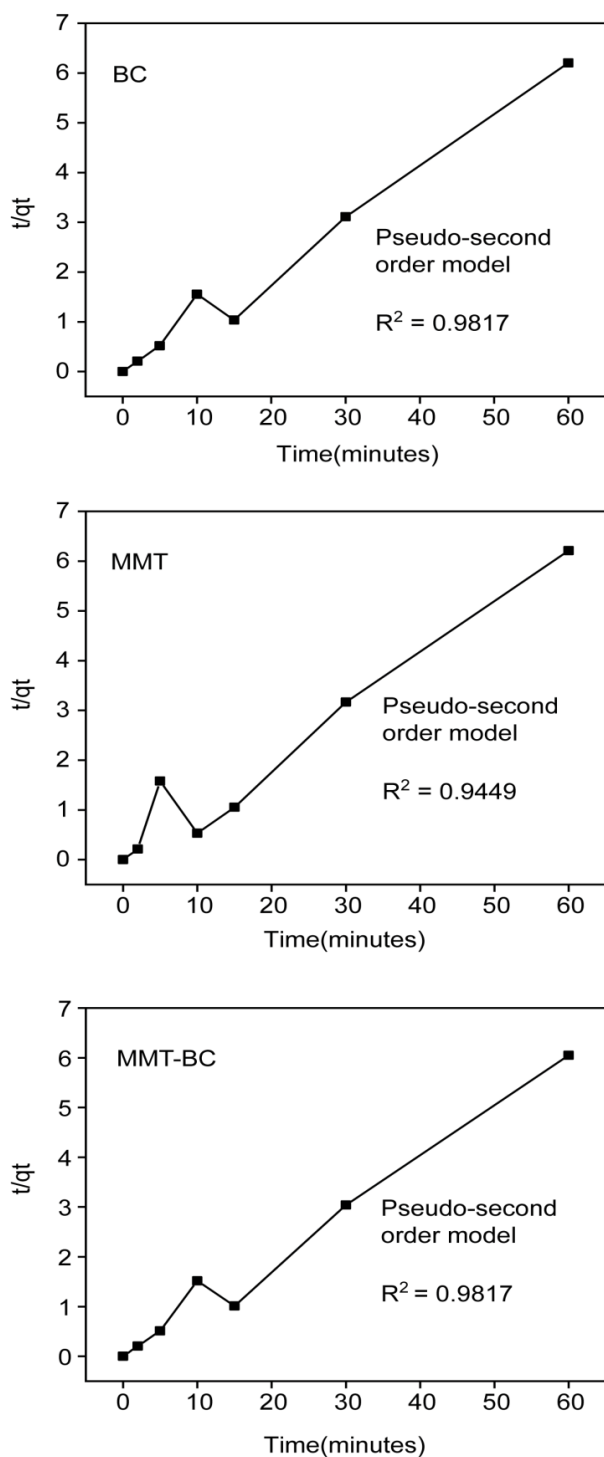
Fig. S11. Linearized form of pseudo-second-order model fitting of BC, MMT and MMT-BC.

increases the movement energy of ions which creates more adsorption sites and enhancing the diffusion of metal ions into the material pore surface [S9]. The linear increase between temperature and adsorption amount proposes that Tl (I) was enabled to diffuse the adsorbent's layer and accumulated in its surface through integration of energy gained at higher reaction temperature [S10]. Subsequently, other experiments done in this study were conducted at 25°C (room temperature).

References

[S1] Y.C. López, G.A. Ortega, M.A. Martínez, E. Reguera, Magnetic Prussian Blue derivative like absorbent cages for an efficient thallium removal, J. Cleaner Prod., 283 (2021), doi: 10.1016/j.jclepro.2020.124587.

[2] H.M. Deng, Y.H. Chen, H.H. Wu, T. Liu, Y.L. Wang, G.Y. Wu, H.P. Ye, Adsorption of Tl (I) on Na–montmorillonite and kaolinite from aqueous solutions, Environ. Earth Sci., 75 (2016), doi: 10.1007/s12665-016-5570-0.

[3] A. Bashir, T. Manzoor, L.A. Malik, A. Qureashi, A.H. Pandith, Enhanced and selective adsorption of Zn(II), Pb(II), Cd(II), and Hg(II) ions by a dumbbell- and flower-shaped potato starch phosphate polymer: a combined experimental and DFT calculation study, ACS Omega, 5 (2020) 4853–4867.

[4] S. Afroze, T.K. Sen, M. Ang, H. Nishioka, Adsorption of methylene blue dye from aqueous solution by novel biomass *Eucalyptus sheathiana* bark: equilibrium, kinetics, thermodynamics and mechanism, Desal. Water Treat., 57 (2016) 5858–5878.

[5] J. Liu, S. Ren, J. Cao, D.C.W. Tsang, J. Beiyuan, Y. Peng, F. Fang, J. She, M. Yin, N. Shen, J. Wang, Highly efficient removal of thallium in wastewater by $MnFe_2O_4$-biochar composite, J. Hazard. Mater., 401 (2021) 123311, doi: 10.1016/j.jhazmat.2020.123311.

[6] S. Gupta, S. Sireesha, I. Sreedhar, C.M. Patel, K.L. Anitha, Latest trends in heavy metal removal from wastewater by biochar based sorbents, J. Water Process Eng., 38 (2020) 101561, doi: 10.1016/j.jwpe.2020.101561.

[7] K. Kuśmierek, A. Świątkowski, The influence of different agitation techniques on the adsorption kinetics of 4-chlorophenol on granular activated carbon, React. Kinet. Mech. Catal., 116 (2015) 261–271.

[8] B. Priyadarshini, P.P. Rath, S.S. Behera, S.R. Panda, T.R. Sahoo, P.K. Parhi, Kinetics, Thermodynamics and Isotherm studies on adsorption of Eriochrome Black-T from aqueous solution using rutile TiO_2, IOP Conf. Ser.: Mater. Sci. Eng., 310 (2018), doi: 10.1088/1757-899X/310/1/012051.

[9] H. Li, X. Li, Y. Chen, J. Long, G. Zhang, T. Xiao, P. Zhang, C. Li, L. Zhuang, W. Huang, Removal and recovery of thallium from aqueous solutions via a magnetite-mediated reversible adsorption–desorption process, J. Cleaner Prod., 199 (2018) 705–715.

[10] J. Song, S. Zhang, G. Li, Q. Du, F. Yang, Preparation of montmorillonite modified biochar with various temperatures and their mechanism for Zn ion removal, J. Hazard. Mater., 391 (2020) 121692, doi: 10.1016/j.jhazmat.2019.121692.